

# CSI-EPT: A novel Contrast Source approach to MRI based Electric Properties Tomography and patient-specific SAR

E. Balidemaj\* J. Trinks\* C. A. T. van den Berg† A. J. Nederveen\*  
A. L. van Lier† L. J. A. Stalpers\* J. Crezee\* R.F. Remis‡

**Abstract** — In this paper, we present a novel method (Contrast Source Inversion - Electric Properties Tomography or CSI-EPT) to dielectric imaging of biological tissue using so-called  $B_1^+$  data measurable by Magnetic Resonance Imaging (MRI) systems. Integral representations for the electromagnetic field quantities are taken as a starting point and we follow an iterative contrast source inversion approach to retrieve the dielectric tissue parameters from measured field data. Numerical results illustrate the performance of the method and show that reliable results are produced near tissue boundaries as opposed to the currently used methods. Fine structures can be resolved as well and since CSI-EPT reconstructs the electric field strength inside a scanning region of interest, it is also a promising candidate to determine the patient-specific SAR deposition during an MRI scan.

## 1 INTRODUCTION

Interest in the electrical properties (conductivity and permittivity) of biological tissues has increased recently as they are essential to determine the specific absorption rate (SAR) and various other electromagnetic field effects that can take place during an MRI scan and Hyperthermia treatment [1].

Various studies have shown that using an MRI system it is feasible to retrieve the electric tissue parameters from measurable so-called transmit  $B_1^+$  field inhomogeneities. The  $B_1^+$  field is the magnetic field component emitted by the RF coil that effectively rotates spins. Rotation of the spins results in a measurable NMR signal. Haacke *et al.* [2] proposed the idea of extracting the tissue parameters from MR data already in 1991. More recently, Katscher *et al.* [3] introduced Electric Property Tomography (EPT) as a means of retrieving the conductivity and permittivity of different tissue types.

\*Radiotherapy and Radiology Departments, University of Amsterdam, Academic Medical Center, Amsterdam, The Netherlands, e-mail: e.balidemaj@amc.nl.

†Radiotherapy Department, Utrecht University, University Medical Center, Utrecht, The Netherlands, e-mail: C.A.T.vandenBerg@umcutrecht.nl

‡Circuits and Systems Group, Faculty of Electrical Engineering, Mathematics and Computer Science, Delft University of Technology, Delft, The Netherlands, e-mail: R.F.Remis@tudelft.nl.

Van Lier *et al.* [4] demonstrated the feasibility of EPT using phase only information and Sodickson *et al.* [5] introduced the so-called Local Maxwell Tomography (LMT) technique, which is free of assumptions on the  $B_1^+$  phase.

What these currently used methods have in common is that local field equations (Maxwell's equations or Helmholtz's equation) are used as a basis for tissue parameter retrieval. The electromagnetic boundary conditions are not taken into account and therefore unreliable results may be produced especially near interfaces between different tissue types. Both methods are also sensitive to noise, since spatial differentiation operators act on generally noisy measured  $B_1^+$  data.

In this paper a novel approach (Contrast Source Inversion - Electric Properties Tomography or CSI-EPT) to tissue parameter retrieval is presented which is based on the Contrast Source Inversion (CSI) method as introduced by Van den Berg, Kleinman, and Abubakar [6, 7]. As opposed to the local methods mentioned above, CSI-EPT takes the global integral representations for the electromagnetic field quantities as a starting point. The boundary conditions are then automatically taken into account and the method is less sensitive to noise since integral operators (instead of differential operators) act on the measured field data. In addition, in an MRI system one is able to measure the  $B_1^+$  fields inside the object of interest whereby each voxel represents a receiving antenna. We therefore expect that CSI-EPT can provide us with high-accuracy dielectric tissue maps of interior parts of the human body. Finally, CSI-EPT reconstructs the unknown electric field as well and is therefore a promising method to determine the patient-specific SAR (Specific Absorption Rate) deposition.

## 2 BASIC EQUATIONS

In the CSI-EPT method, we take the domain integral representations

$$H_j^{sc}(\mathbf{x}) = \eta \int_{\mathbf{x}' \in \mathbb{D}} G_{j,r}^{HJ}(\mathbf{x}, \mathbf{x}') w_r(\mathbf{x}') dV \quad (1)$$

and

$$E_k^{\text{sc}}(\mathbf{x}) = \eta \int_{\mathbf{x}' \in \mathbb{D}} G_{k,r}^{\text{EJ}}(\mathbf{x}, \mathbf{x}') w_r(\mathbf{x}') dV \quad (2)$$

as a starting point. Here we use subscript notation and the Einstein summation convention applies. The domain  $\mathbb{D}$  is the imaging domain of interest and both representations hold for all points  $\mathbf{x} \in \mathbb{R}^3$ . Furthermore,  $\eta = \sigma + j\omega\varepsilon$ , where  $\sigma$  and  $\varepsilon$  are the conductivity and permittivity of the background medium, while  $G_{j,r}^{\text{HJ}}$  and  $G_{k,r}^{\text{EJ}}$  are the electric-current to magnetic field and electric-current to electric field Green's tensors, respectively. Finally,  $w_r = \chi(\mathbf{x})E_r(\mathbf{x})$  is the so-called contrast source, where  $\chi(\mathbf{x}) = \eta^{\text{sc}}/\eta - 1$  is the contrast function and  $\eta^{\text{sc}}(\mathbf{x}) = \sigma^{\text{sc}}(\mathbf{x}) + j\omega\varepsilon^{\text{sc}}(\mathbf{x})$ , where  $\sigma^{\text{sc}}(\mathbf{x})$  and  $\varepsilon^{\text{sc}}(\mathbf{x})$  are the conductivity and permittivity of the object under test.

As mentioned above, in an MRI system the so-called  $B_1^+$  field can be measured inside the scattering object. With a static background  $B_0$  field directed in the positive  $x_3$ -direction, this field is given by

$$\mathcal{B}_1^+(\mathbf{x}) = \frac{B_1(\mathbf{x}) + jB_2(\mathbf{x})}{2}$$

where  $\mathbf{x} \in \mathbb{S}$  and  $\mathbb{S}$  is the domain in which the  $B_1^+$  field is measured. Since the incident magnetic field is known, the corresponding scattered  $B_1^+$  field can be found through measurement as well. Using the integral representation of Eq. (1), this scattered field can be written as

$$\mathcal{B}_1^{+;\text{sc}}(\mathbf{x}) = G_S\{w_r\}(\mathbf{x}), \quad (3)$$

where we have introduced the  $B_1^+$  data operator  $G_S$  as

$$\begin{aligned} G_S\{w_r\}(\mathbf{x}) = \\ \frac{1}{2}\mu_0\eta \int_{\mathbf{x}' \in \mathbb{D}} [G_{1,r}^{\text{HJ}}(\mathbf{x}, \mathbf{x}') + jG_{2,r}^{\text{HJ}}(\mathbf{x}, \mathbf{x}')] w_r(\mathbf{x}') dV, \end{aligned} \quad (4)$$

with  $\mathbf{x} \in \mathbb{S}$ . Equation (3) is known as the *data equation*. It relates the scattered  $B_1^+$  field to the contrast source  $w_r$  via the electric-current to magnetic field Green's tensor  $G_{j,r}^{\text{HJ}}$  of the background medium.

The contrast source consists of a product of the contrast function and the total electric field strength inside the body. Both quantities are unknown, of course, but we do know that Eq. (2) should hold inside the body under test. Specifically, with  $E_k^{\text{sc}} = E_k - E_k^{\text{inc}}$ , where  $E_k^{\text{inc}}$  is the electric field strength in the background medium, we must have

$$E_k(\mathbf{x}) - \eta \int_{\mathbf{x}' \in \mathbb{D}} G_{k,r}^{\text{EJ}}(\mathbf{x}, \mathbf{x}') w_r(\mathbf{x}') dV = E_k^{\text{inc}}(\mathbf{x}) \quad (5)$$

with  $\mathbf{x} \in \mathbb{D}$ . This equation is known as the *object equation*. Introducing the object operator

$$G_{D;k}\{w_r\}(\mathbf{x}) = \eta \int_{\mathbf{x}' \in \mathbb{D}} G_{k,r}^{\text{EJ}}(\mathbf{x}, \mathbf{x}') w_r(\mathbf{x}') dV, \quad (6)$$

with  $\mathbf{x} \in \mathbb{D}$ , we can write the object equation as

$$w_k(\mathbf{x}) - \chi(\mathbf{x})G_{D;k}\{w_r\}(\mathbf{x}) = \chi(\mathbf{x})E_k^{\text{inc}}(\mathbf{x}), \quad (7)$$

$\mathbf{x} \in \mathbb{D}$ , where we have multiplied by the contrast function as well.

Now for a given contrast source, we measure the discrepancy in satisfying the data equation (3) via the data residual  $\rho(\mathbf{x}) = \mathcal{B}_1^{+;\text{sc}}(\mathbf{x}) - G_S\{w_r\}(\mathbf{x})$ , where  $\mathbf{x} \in \mathbb{S}$ . Similarly, for a given contrast  $\chi$  and contrast source  $w_r$  we define the residual that corresponds to the object equation (7) as  $r_k(\mathbf{x}) = \chi(\mathbf{x})E_k(\mathbf{x}) - w_k(\mathbf{x})$ , where  $\mathbf{x} \in \mathbb{D}$ . With the introduction of these data and object residuals, we now define the objective function

$$F(w_r, \chi) = \frac{\|\rho(\mathbf{x})\|_S^2}{\|\mathcal{B}_1^{+;\text{sc}}(\mathbf{x})\|_S^2} + \frac{\|r_k(\mathbf{x})\|_D^2}{\|\chi(\mathbf{x})E_k^{\text{inc}}(\mathbf{x})\|_D^2}, \quad (8)$$

where

$$\|\rho(\mathbf{x})\|_S^2 = \int_{\mathbf{x}' \in \mathbb{S}} |\rho(\mathbf{x}')|^2 dV \quad (9)$$

is the squared magnitude of the data residual and

$$\|r_k(\mathbf{x})\|_D^2 = \int_{\mathbf{x}' \in \mathbb{D}} r_k(\mathbf{x}') \bar{r}_k(\mathbf{x}') dV \quad (10)$$

is the squared magnitude of the object residual. In the above equation, the overbar denotes complex conjugation.

To retrieve the tissue parameters from the measured data, the objective function is minimized by iteratively updating the contrast source and contrast function. Specifically, with  $\chi^{[n-1]}$  and  $w_r^{[n-1]}$  known, we first keep the contrast function fixed and update the contrast source using the update formula  $w_r^{[n]} = w_r^{[n-1]} + \alpha^{[n]}v_r^{[n]}$ , where  $\alpha^{[n]}$  is called the step length and  $v_r^{[n]}$  is the Polak-Ribière conjugate gradient direction. In particular, we have  $v_r^{[0]} = 0$  and

$$v_r^{[n]} = g_r^{[n]} + \frac{\text{Re}\langle g_k^{[n]}, g_k^{[n]} - g_k^{[n-1]} \rangle_D}{\|g_k^{[n-1]}\|_D^2} v_r^{[n-1]},$$

for  $n \geq 1$ , where  $\langle \cdot, \cdot \rangle_D$  is the inner product on  $\mathbb{D}$  that induces the norm given by Eq. (10) and  $g_k^{[n]}$  is the gradient of the objective function with respect

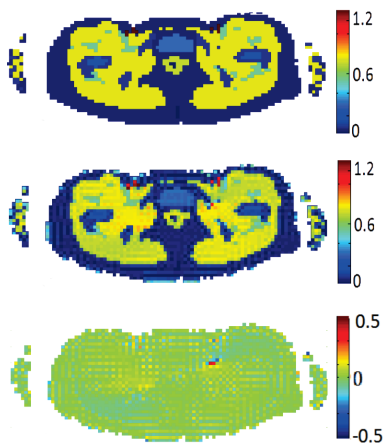


Figure 1: Original conductivity map of pelvic region (top) and the reconstructed conductivity map after 5000 iterations of the CSI-EPT method (middle). The difference map is shown at the bottom.

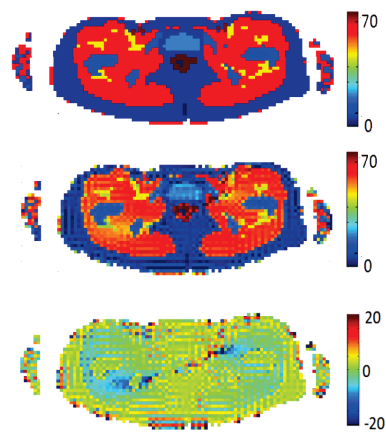


Figure 2: Original permittivity map of pelvic region (top) and the reconstructed permittivity map after 5000 iterations of the CSI-EPT method (middle). The difference map is shown at the bottom.

to  $w_r$ . This gradient is given by

$$g_k^{[n]} = -\frac{G_{S;k}^*\{\rho^{[n-1]}\}}{\|\mathcal{B}_1^{+;sc}(\mathbf{x})\|_S^2} - \frac{r_k^{[n-1]} - G_{D;k}^*\{\bar{\chi}^{[n-1]}r_r^{[n-1]}\}}{\|\chi^{[n-1]}(\mathbf{x})E_k^{inc}(\mathbf{x})\|_D^2},$$

where  $G_{S;k}^*$  and  $G_{D;k}^*$  are the adjoints of the operators  $G_S$  and  $G_D$ , respectively. Finally,  $\alpha^{[n]}$  is determined by minimizing the objective function with respect to the step length.

Having the new contrast source available, we subsequently find a new contrast function by fixing the contrast source to  $w_r^{[n]}$ , setting  $\chi = \chi^{[n-1]}$  in the denominator of the second term in Eq. (8), and minimizing the nominator of this second term with respect to the contrast function. After this minimization step, the contrast source and contrast function have both been updated and the process is repeated until a specified error criterion is met. Further details about the updating scheme can be found in [7], for example. We do mention here, however, that back-projected data is used as an initial guess for the contrast source  $w_r^{[0]}$ . The corresponding field  $E_r^{[0]}$  is then computed using the object equation and the initial guess for the contrast  $\chi^{[0]}$  follows from minimizing the difference between  $w_r^{[0]}$  and  $\chi^{[0]}E_r^{[0]}$  as measured by the norm defined over the domain  $\mathbb{D}$  (see Eq. (10)).

### 3 NUMERICAL RESULTS

To illustrate the performance of the CSI-EPT method, we consider a two-dimensional configura-

tion in which E-polarized waves are present. According to [8], such fields provide a good approximation of the fully vectorial three-dimensional field inside a pelvic region that is situated in the mid-plane of a 3T body coil. We therefore take a slice from a female pelvis model (Ella model, IT'IS foundation, see Figs. 1 and 2 (top)) and use this model as a test for the CSI-EPT method. A homogeneous medium is taken as a background model (no RF shield is taken into account) and the conductivity and permittivity values are for an operating frequency of 128 MHz [9], which corresponds to the operating frequency of the RF body coil in 3T MRI systems.

A forward modeling code is used to compute the  $B_1^+$  field inside the pelvis model. This field is emitted by eight line sources symmetrically located around the object and driven at  $f = 128$  MHz in a quadrature setting to mimic a realistic body-coil used in MRI systems. Furthermore, exact knowledge of  $B_1^+$  phase is assumed. In practice, however, measurements of the  $B_1^+$  phase are based on assumptions regarding the object and coil geometry [3, 4].

Having the  $B_1^+$  field inside the human anatomy model available, we now use it as an input for the CSI-EPT method. The reconstructed conductivity and permittivity maps obtained after 5000 iterations are shown in Figs. 1 and 2 (middle), respectively, while the corresponding difference maps (difference between the original and reconstructed profiles) are shown at the bottom of these figures. We observe that the conductivity and permittivity profile reconstructions are highly accurate. Fine structures are resolved and the method produces

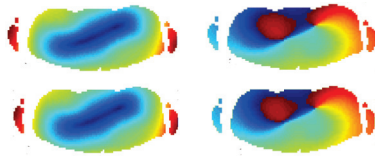


Figure 3: Normalized magnitude and phase of the electric field corresponding to the original Ella model (top row) and the magnitude and phase of the reconstructed electric field (bottom row).

reliable results near interfaces between different tissue types.

In the top row of Fig. 3 we also show the electric field amplitude and phase that correspond to the original conductivity and permittivity maps of the Ella model. The reconstructed electric field magnitude and phase obtained after 5000 iterations of the CSI-EPT method are shown in the bottom row of Fig. 3. This example clearly illustrates the ability of CSI-EPT to reconstruct the electric fields quite accurately and opens up the possibility of true patient specific SAR determination based on  $B_1^+$  measurements. Finally, we mention that for this problem 5000 iterations of a Matlab implementation of the CSI-EPT method takes about two minutes on an Intel Core Quad 2.83Ghz.

#### 4 DISCUSSION AND CONCLUSION

In this paper, we have presented a contrast source inversion approach to electric property mapping in MRI. The method takes the integral representations for the electromagnetic field as a starting point and the tissue parameters are obtained by iteratively minimizing an objective function which measures the discrepancy between measured and modeled data and the discrepancy in satisfying a consistency equation known as the object equation. Numerical results illustrate that fine structures can be resolved and the method can handle large jumps in the tissue parameters as well.

The applicability of the basic CSI-EPT method to electric property mapping has recently been confirmed in a series of experiments with phantom models in a 3T MRI scanner. In its present form, however, CSI-EPT does not include any additional regularization terms to suppress the effects of noise. Up till now, the iteration parameter serves as a regularization parameter, but then usually smooth reconstruction results are obtained. Future work therefore focuses on the implementation of  $L_1$  and  $L_2$  regularization schemes and the inclusion of *a priori* information via positivity constraints, for example.

#### Acknowledgments

The research presented in this paper was supported by the Dutch Cancer Society (Grant number: UVA 2010-4660).

#### References

- [1] M. de Greef, H. P. Kok, D. Correia, A. Bel, and J. Crezee, "Uncertainty in hyperthermia treatment planning: the need for robust system design," *Physics in Medicine and Biology*, Vol. 56, No. 11, pp. 3233-3250, 2011.
- [2] E. M. Haacke, L. S. Petropoulos, E. W. Nilges, and D. H. Wu, "Extraction of conductivity and permittivity using magnetic resonance imaging," *Physics in Medicine and Biology*, Vol. 36, No. 6, pp. 723-734, 1991.
- [3] U. Katscher, T. Voigt, C. Findekklee, P. Vernickel, K. Nehrke, and O. Dössel, "Determination of electric conductivity and local SAR via  $B_1$  mapping," *IEEE Trans Med Imag*, Vol. 28, No. 9, 1365-75, 2009.
- [4] A. L. Van Lier, D. O. Brunner, K. P. Pruessmann, D. W. Klomp, P. R. Luijten, J. J. Lagendijk, and C. A. T. van den Berg, " $B_1^+$  phase mapping at 7 T and its application for in vivo electrical conductivity mapping," *Magnetic Resonance in Medicine*, Vol. 67, No. 2, pp. 552-561, 2011.
- [5] D. K. Sodickson, L. Alon, C. M. Deniz, N. Ben Elizier, M. A. Kloos, L. A. Sodickson, C. M. Collins, G. C. Wiggins, and D. S. Novikov "Generalized local Maxwell tomography for mapping of electrical property gradients and tensors," *Proc. ISMRM 2013*, 4175, 2013.
- [6] P. M. Van den Berg and R. E. Kleinman, "A contrast source inversion method," *Inverse Problems*, Vol. 13, pp. 1607 – 1620, 1997.
- [7] P. M. Van den Berg and A. Abubakar, "Contrast source inversion method: state of art," *Progress in Electromagnetics Research*, Vol. 34, pp. 189 – 218, 2001.
- [8] B. Van den Bergen, C. C. Stolk, J. B. van den Berg, J. J. W. Lagendijk, and C. A. T. van den Berg, "Ultra fast electromagnetic field computations for RF multi-transmit techniques in high field MRI," *Physics in Medicine and Biology*, Vol. 54, No. 5, pp. 1253-1264, 2009.
- [9] C. G. Gabriel and E. Corthout, "The dielectric properties of biological tissues: I. Literature survey," *Physics in Medicine and Biology*, Vol. 41, pp. 2231-2249, 1996.